NANO · MICRO small
www.small-journal.com

Highly Fluorinated Peptide Probes with Enhanced In Vivo Stability for ^{19}F-MRI

Beibei Meng, Stephan L. Grage, Oleg Babii, Masanari Takamiya, Neil MacKinnon, Tim Schober, Illia Hutskalov, Omar Nassar, Sergii Afonin, Serhii Koniev, Igor V. Komarov, Jan G. Korvink, Uwe Strähle, and Anne S. Ulrich**

A labeling strategy for in vivo ^{19}F-MRI (magnetic resonance imaging) based on highly fluorinated, short hydrophilic peptide probes, is developed. As dual-purpose probes, they are functionalized further by a fluorophore and an alkyne moiety for bioconjugation. High fluorination is achieved by three perfluoro-*tert*-butyl groups, introduced into asparagine analogues by chemically stable amide bond linkages. D-amino acids and *β*-alanine in the sequences endow the peptide probes with low cytotoxicity and high serum stability. This design also yielded unstructured peptides, rendering all 27 ^{19}F substitutions chemically equivalent, giving rise to a single ^{19}F-NMR resonance with <10 Hz linewidth. The resulting performance in ^{19}F-MRI is demonstrated for six different peptide probes. Using fluorescence microscopy, these probes are found to exhibit high stability and long circulation times in living zebrafish embryos. Furthermore, the probes can be conjugated to bovine serum albumin with only amoderate increase in ^{19}F-NMR linewidth to ≈30 Hz. Overall, these peptide probes are hence suitable for in vivo ^{19}F-MRI applications.

1. Introduction

In vivo imaging of fluorine-containing compounds is of high medical relevance as nearly 30% of the newly approved drugs contain at least one fluorine,[1] half of which carry a CF_3 group.[2,3] Fluorine is often selectively incorporated into the structure of a candidate small-molecule therapeutic to modulate the physicochemical properties and improve metabolic stability.[4,5] Due to its high gyromagnetic ratio and absence of natural background signal, ^{19}F has been used as a highly sensitive label for NMR spectroscopy,[6,7] for example, to study self-assembly of peptides on lipid membranes,[8] dynamics of receptors,[9] and tracking of drug molecules in cells.[10] Furthermore, the favorable properties of ^{19}F have been exploited in magnetic resonance imaging (MRI) already in the 1970s.[11] Unlike the abundant protons (^{1}H), ^{19}F allows selective labeling and, therefore, high contrast in imaging. However, single, double, or even triple ^{19}F probes as used in ^{19}F-NMR spectroscopy are insufficient in MRI, and a higher local ^{19}F concentration is required to overcome the low sensitivity. To resolve this restriction, the most straightforward strategy is to increase the amount of fluorine in a single molecule.

B. Meng, T. Schober, I. Hutskalov, A. S. Ulrich
Institute of Organic Chemistry (IOC)
Karlsruhe Institute of Technology (KIT)
Fritz-Haber-Weg 6, 76131 Karlsruhe, Germany
E-mail: anne.ulrich@kit.edu

S. L. Grage, O. Babii, S. Afonin, S. Koniev, A. S. Ulrich
Institute of Biological Interfaces (IBG-2)
KIT
POB 3640, 76021 Karlsruhe, Germany
E-mail: stephan.grage@kit.edu

M. Takamiya, U. Strähle
Institute of Biological and Chemical Systems (IBCS) – Biological Information Processing
KIT
Karlsruhe, Germany

N. MacKinnon, O. Nassar, J. G. Korvink
Institute of Microstructure Technology (IMT)
KIT
Karlsruhe, Germany

N. MacKinnon
Karlsruhe Nano Micro Facility (KNFMi)
KIT
Karlsruhe, Germany

S. Koniev
Lumobiotics
Karlsruhe, Germany

I. V. Komarov
Taras Shevchenko National University of Kyiv
Kyiv, Ukraine

T. Schober, S. Koniev, I. V. Komarov
Enamine
Kyiv, Ukraine

The ORCID identification number(s) for the author(s) of this article can be found under https://doi.org/10.1002/smll.202107308.

DOI: 10.1002/smll.202107308

Consequently, perfluorocarbons were applied in the first ^{19}F-MRI experiments,[11] and to date, are used in many applications,[12] such as angiogenesis imaging,[13] visualization of inflammation,[14] immune cell cancer therapy,[15] hepatic uptake,[16] activatable targeting,[17,18] and theranostics.[19,20] However, because of their extremely high hydrophobicity, the use of perfluorocarbons relies on the construction of nanoparticles with hydrophilic shells in order to achieve biocompatibility, which may cause retention and stability problems in the body.[21] Another approach has employed liposomal formulations of hydrophilic fluorine-rich organic compounds to overcome the hydrophobicity.[22] As an alternative with tunable hydrophilicity, peptide-based ^{19}F-MRI probes have been suggested. Kirberger et al., for example, have reported peptide probes composed of alternating trifluoro-acetylated L-lysines (TFA-lysine) and D-lysines to endow the peptide with stability against proteolysis.[23] Nonetheless, stability beyond ≈24 h has still been an issue due to slow hydrolysis of the trifluoroacetamide bond at physiological pH. In their study the authors chose the amino acid sequence to obtain an unfolded peptide in aqueous environment, which lead to an identical chemical shift of all ^{19}F-labels. Avoiding secondary structure and hence chemical shift dispersion assured a high intensity in ^{19}F-NMR and therefore increased the detectability in ^{19}F-MRI.

Our study intended to develop hydrolytically and proteolytically stable peptide probes and increase the number of ^{19}F even further, as signal intensity is the major challenge in ^{19}F-MRI. However, a mere extension of the peptide length bears the risk that the peptide will eventually adopt a secondary structure, leading to a spread in local environments and hence ^{19}F chemical shift. Equally, a larger size of the peptide probe can influence the biological activity of any labeled biomolecule. In order to realize a short peptide probe with nonetheless maximized ^{19}F signal while keeping its size compact, we used perfluoro-*tert*-butyl groups as functional units to label several amino acids in a peptide. Each moiety possesses nine fluorine atoms, thus yielding a threefold higher signal as compared to commonly used CF_3 labels. As in the case of CF_3, all ^{19}F atoms in a perfluoro-*tert*-butyl group are chemically equivalent due to their rapid axial rotation on the NMR-time scale,[24] contributing additionally to an intense signal in ^{19}F-MRI. Furthermore, the additional hydrophobicity introduced by the high fluorination was compensated by the incorporation of polar amino acids in the peptides, as well as by endowing the fluorinated amino acid with multiple polar groups. A similar approach has been followed by Taylor et al., who used polymers containing nonafluorooxy-ethylacrylate and poly(ethylene glycol) acrylate units to tune the hydrophilicity.[25] Compared to partially fluorinated polymers, using peptide-based ^{19}F-MRI probes offers better control on the synthesis, leading to a platform that allows more precise tuning of spectroscopic properties and generating well-defined products with higher biocompatibility.

In this paper, we describe six fluorinated peptide probes employing perfluoro-*tert*-butyl groups as ^{19}F labels, which boost the magnetic resonance signal of ^{19}F by massive fluorination. The hydrophobicity associated with fluorination is overcome by introducing multiple cationic or anionic residues, and proteolytic degradation of the peptides in vivo is decreased by including D-amino acids and β-alanine in the sequence. Currently, only a few perfluoro-*tert*-butyl amino acids have been published, such as serine, homoserine, tyrosine, and hydroxyproline analogues synthesized through the functionalization of an OH group.[24,26–28] For the first time, here we introduce a perfluoro-*tert*-butyl moiety into aspartic acid to form an asparagine analogue (Asn^{F9}) with nine magnetically equivalent fluorine atoms. In this amino acid, the fluorinated moiety is connected via a sufficiently long linker, not only to reduce susceptibility to racemization (which the electronegative fluorine nucleus may cause), but also to distance the bulky C_4F_9 group from the carboxylate to maintain a high reactivity during peptide synthesis. In addition, we aimed for favorable relaxation properties due to the high mobility of the C_4F_9 group at the end of the elongated side chain.

We connected a nonafluoro-*tert*-butyl precursor to the aspartic acid side chain via an amide bond. For this, we chose ethanolamine as a linker between the amino acid fragment and the fluorine-rich moiety. The resulting sterically hindered amide bond is unlikely to be hydrolyzed or enzymatically cleaved under physiological conditions. The final perfluoro-*tert*-butyl containing α-amino acid derivative **6** (Asn^{F9}) was obtained in only four steps from commercially available starting materials using standard chemistry protocols (**Figure 1**, Scheme S1 and Figures S1–S9, Supporting Information). Starting from *N*-Boc (*tert*-butoxycarbonyl) ethanolamine **1**, precursor **3** was obtained via previously described Mitsunobu reaction[29] with nonafluoro-*tert*-butanol and subsequent Boc-deprotection of the intermediate **2**. 1-*tert*-butyl-ester *N*-Fmoc (fluorenylmethoxycarbonyl) protected aspartic acid **4** was coupled to precursor **3** using amide coupling reagent PyAOP ((7-azabenzotriazol-1-yloxy)tripyrrolidinophosphonium hexafluorophosphate) in the presence of base to obtain intermediate **5**. Final trifluoroacetic acid (TFA)-mediated cleavage of the *tert*-butyl protection gave product **6** (*N*-Fmoc-Asn^{F9}) with an overall yield of 28%, suitable for solid-phase peptide synthesis.

Ideally, our goal is to obtain a single narrow ^{19}F-NMR resonance, which can be achieved if all CF_3 groups are in an essentially identical chemical environment. To this aim, our design of the peptides avoids any secondary structure and places all ^{19}F labels in identical repeat units. The resulting four peptide probes (P1–P4) consist of three identical repeat units—each of which carries a fluorinated Asn^{F9} and a charged amino acid—plus two further amino acids at the *N*-terminus for fluorescent labeling and bioconjugation (**Table 1** and structures in Figure S10, Supporting Information). In addition, to investigate the influence of the peptide length on the ^{19}F-NMR signal, P5 and P6 have been synthesized as short probes with only a single repeat unit.

The amino acids in the repeat unit were selected considering the following peptide properties allowing an optimized use for in vivo ^{19}F-MRI: 1) high solubility, 2) prevention of secondary structure, 3) proteolytic stability, 4) tag for bioconjugation, and 5) fluorescence label.

1) High water-solubility was achieved by including D-lysine or D-glutamic acid as cationic or anionic amino acids. 2) A mixture of D- and L-amino acid stereoisomers was chosen to prevent the formation of α-helical secondary structures. This way, we envisaged to avoid peptide folding, and therefore prevent different ^{19}F-NMR chemical shifts and hence multiple NMR

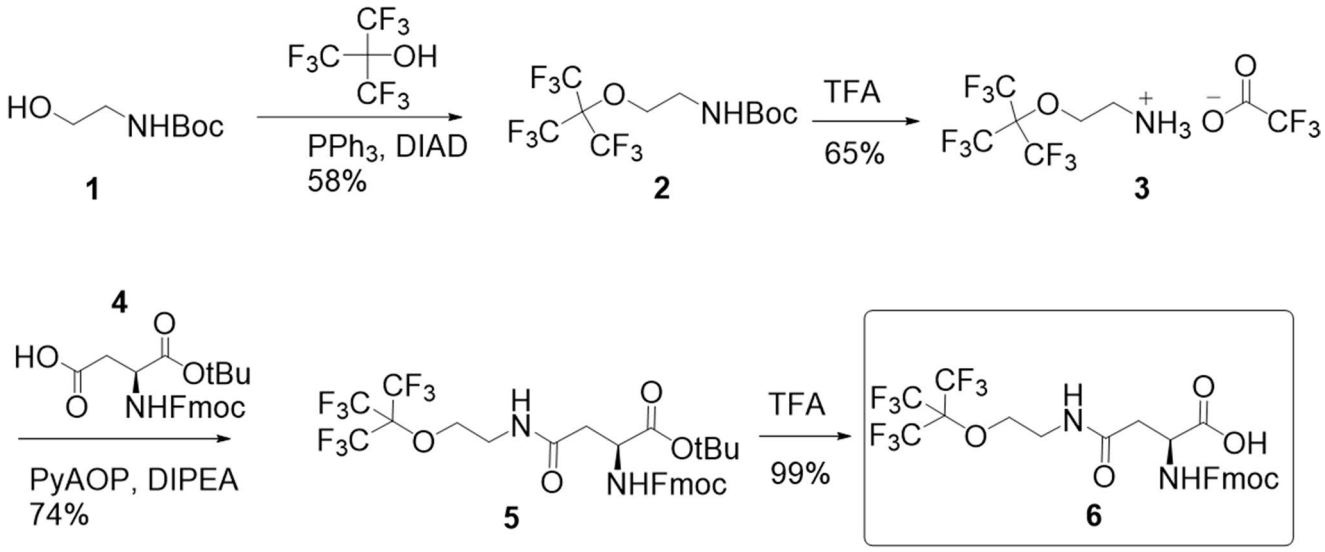

Figure 1. Synthesis of Fmoc-protected Asn^{F9}. Percentages represent the yields of the respective synthesis steps.

signals. In addition, *β*-alanine was included in the repeat unit of P1 and P3 to evaluate a possible improvement of the backbone flexibility of the probes.[30] 3) Importantly, D-amino acids also offer a stronger resistance against proteolytic degradation, as many enzymes only recognize the naturally abundant L-isomers. 4) Furthermore, we introduced a propargylglycine with an alkyne function, in order to allow coupling of other molecules to the peptide via "click" reaction on the *N*-terminal side of the peptides. 5) To monitor the peptide distribution in zebrafish embryos using fluorescence microscopy, we attached rhodamine B to the *N*-terminus of aliquots of all peptides in a second series of fluorescent products Rho-P1 to Rho-P6 (Figures S13–S15, Supporting Information). In order to ensure the functionality of the dye in its active open form, a sarcosine was introduced at the *N*-terminus to then be adjacent to the fluorophore.[31] To simplify the synthesis, an additional glycine was added at the *C*-terminus.

2. Results and Discussion

The peptides were synthesized manually on solid support following the standard Fmoc protocol. The identity and purity of the peptide probes were confirmed by mass spectrometry (matrix-assisted laser-induced desorption/ionization, MALDI-MS) and reverse-phase high-performance liquid chromatography (RP-HPLC) (see Table S1 and Figures S11–S12, Supporting Information). We observed a polarity decreasing in the order of P6 > P5 > P3 > P4 > P1 > P2, as can be judged from increasing retention times when eluted by a linear gradient of acetonitrile/water in RP-HPLC (Figure S12, Supporting Information). These results illustrate a decrease in hydrophilicity with increasing number of fluorine atoms per peptide length. Notably, *β*-alanine increased the hydrophilicity of the peptide probes, whereas D-glutamic acid had a smaller contribution to the improvement of the polarity than D-lysine. As the fluorinated peptide probes have different lipophilicity and charge, they are expected to show different biodistribution and pharmacokinetics in vivo.

Table 1. Sequences of peptide probes for ^{19}F-MRI synthesized and explored in this study.

Peptide	Sequence[a)]
P1	Sar-Pra-(Bal-glu-Asn^{F9})$_3$-Gly-OH
P2	Sar-Pra-(glu-Asn^{F9})$_3$-Gly-OH
P3	Sar-Pra-(Bal-lys-Asn^{F9})$_3$-Gly-OH
P4	Sar-Pra-(lys-Asn^{F9})$_3$-Gly-OH
P5	Sar-Pra-glu-Asn^{F9}-Gly-OH
P6	Sar-Pra-lys-Asn^{F9}-Gly-OH

[a)]Sar = sarcosine, Pra = L-propargylglycine, Bal = ß-alanine, glu = D-glutamic acid, lys = D-lysine, Asn^{F9} = perfluoro-*tert*-butyl-modified L-asparagine.

^{19}F-NMR spectroscopy was applied to characterize the probes in terms of how well they will be suited for ^{19}F-MRI. Encouragingly, when dissolved in PBS (phosphate buffer saline, pH 7.4) at a ^{19}F concentration of 5.4 mM, a single resonance or splitting into a set of very close signals (P3) at around –69.3 ppm with a very narrow linewidth of ≈8 Hz was observed for all peptide probes, demonstrating that all fluorine nuclei are in a similar chemical environment (**Figure 2**A, Supporting Information). Furthermore, all peptides, except for P1, were soluble in methanol, where P5 and P6 exhibited single sharp peaks at around –70.7 ppm with the same narrow linewidth as in PBS. The peak splitting of P2–P4 with a slight increase in the chemical shift span in methanol indicates that the ^{19}F labeled side chains are in slightly different environments, possibly due to formation of some local secondary structure or aggregation in the organic solvent. By comparison, the rhodamine-labeled peptides (Rho-peptides) showed a broadening of the ^{19}F-NMR peak in PBS, demonstrating a higher tendency to fold or aggregate (Figure S16, Supporting Information). Their larger linewidth or chemical shift dispersion is presumably related to the more hydrophobic character of the rhodamine-labeled constructs, which is also visible in the longer retention

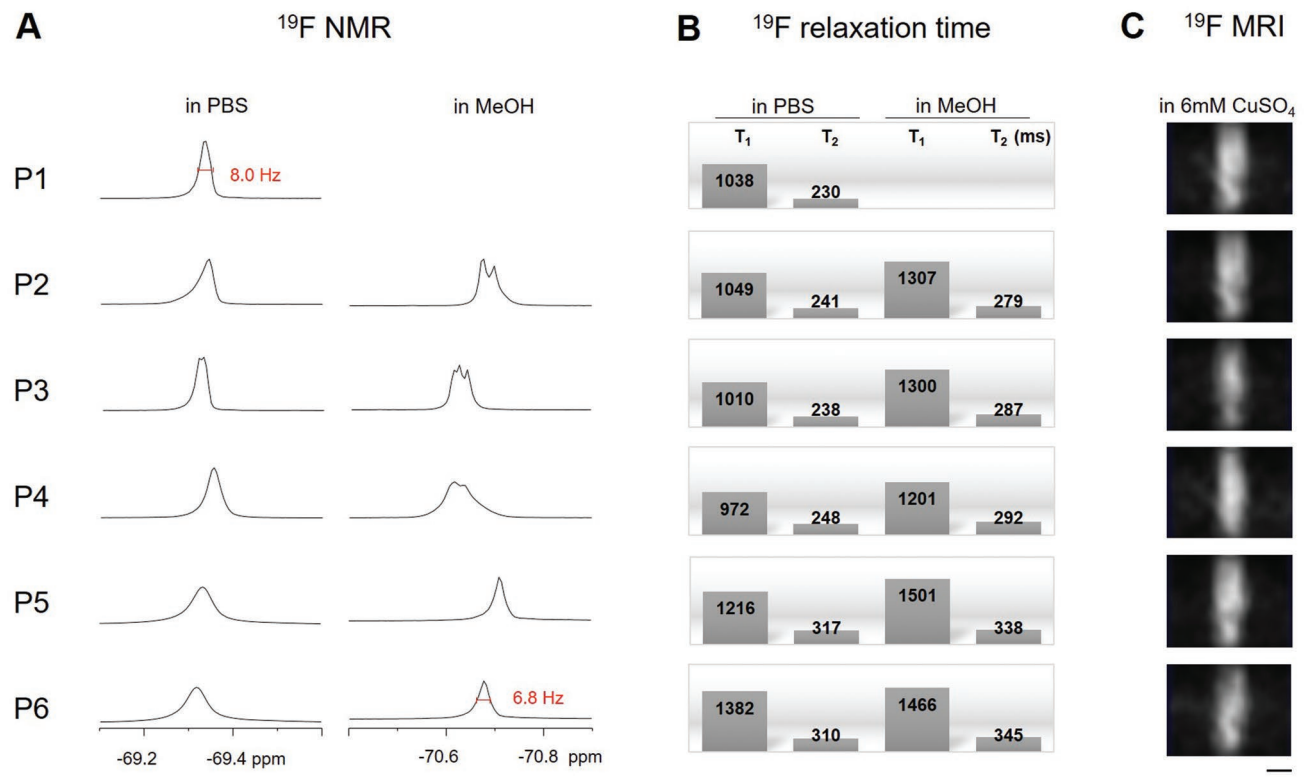

Figure 2. ^{19}F characteristics of peptide probes. A) ^{19}F-NMR spectra of peptides P1–P6 at ^{19}F concentration of 5.4 mM (0.2 mM of P1–P4 and 0.6 mM of P5–P6) in PBS buffer at pH 7.4 (left) and methanol (right). The narrowest peak width at half height for each condition is marked in red. B) ^{19}F relaxation times of the peptides (5.4 mM ^{19}F) in PBS and methanol. C) ^{19}F-MRI of peptide solutions in 6 mM $CuSO_4$ (65 mM NaOH added in P1 and P2 solution for pH adjustment) at ^{19}F concentration of 675 mM (P1–P4 at 25 mM and P5–P6 at 75 mM). The aqueous solutions were filled into capillaries with an inner diameter of 1.6 mm and an outer diameter of 2.0 mm, and fitted into a homemade microcoil.[32] Images of coronal planes were acquired using a Fast Low Angle Shot Gradient Echo (FLASH) sequence with a recycle delay of 5.765 ms, an echo delay of 2.72 ms, and a flip angle of 45°. The images were processed using a smoothing algorithm (binning with an average shrink factor 32) of ImageJ. Scale bar: 1 mm.

times in RP-HPLC and significantly decreased T_2 (Figure S15 and Table S2, Supporting Information).

At a ^{19}F concentration of 5.4 mM, the ^{19}F linewidth of the peptides is found to increase as P1 ≈ P3 < P2 ≈ P4 < P5 ≈ P6, implying that β-alanine leads to a reduction of the effective ^{19}F-NMR linewidth and an increase in signal intensity (Figure 2A). On the other hand, the ^{19}F signal obtained for the shorter peptides P5 and P6, measured at a concentration of 0.6 mM, which corresponds to the same fluorine concentration as for P1–P4, interestingly exhibited slightly broader linewidth and lower intensity than the longer peptides, potentially due to the higher net hydrophobicity of the shorter peptides. In in vivo applications the linewidths may be broadened further due to intermolecular contacts with molecular constituents of the tissue. However, our label design avoids such additional line broadening as we included charged residues in the peptide sequence. As has been reported previously,[23] labels equipped with a high degree of polarity lead to linewidths compatible with ^{19}F MRI also in biological tissue. Hence, using charged residues, as in our case, should avoid intermolecular interactions and line broadening even more. Moreover, our modular design with positively or negatively charged residues provides a range of options allowing to optimize the peptide label with respect of the linewidth.

In addition, we measured T_1 and T_2 ^{19}F-NMR relaxation times to assess the performance of the peptides in ^{19}F-MRI, where a short T_1 and long T_2 value would be desirable. T_1 was found to be in the range of 1.0–1.3 s, which compares well with T_1 of other compounds labeled with trifluoromethyl groups.[22] T_2 values in the range of 200–300 ms were determined, which are longer than typical values for fluorine-labeled molecules of the size of the peptides and hence favorable for ^{19}F-MRI (Figure 2B). We note at this point, that T_2 relaxation is not the only factor contributing to the linewidths (Figure 2A), as apparent from the linewidths exceeding the relaxation-related linewidth estimate of $1/(\pi T_2)$.

We compared the performance of the six peptides as ^{19}F-MRI labels using a microcoil imaging setup operating at 11.7 T.[32] Peptides were dissolved in 6 mM aqueous $CuSO_4$ to enhance T_1 relaxation and decrease the recycle delay mainly to facilitate the setup procedure and in the development process. (We note here, that the usage of shorter flip angles in the FLASH imaging sequence reduces the necessity of signal recovery by T_1 relaxation.[33]) The peptide concentrations, 25 mM in the case of P1–P4 and 75 mM in the case of P5–P6, were adjusted to achieve a fluorine concentration of 675 mM, and NaOH was added in the case of the anionic peptides P1 and P2 to improve their solubility. (Figure 2C). For the images, a volume of

7 mm × 7 mm × 5 mm divided into 32 × 32 × 20 voxels was scanned with 10 240 repetitions in 30 min. All peptides exhibited a similar imaging performance. Only for P3 a slight reduction in intensity was observed, which may be related to the signal dispersion already seen in the ^{19}F-NMR spectra. Hence, we have demonstrated here the use of our peptide-based probes in in vitro ^{19}F-MRI on a submillimeter-scale, which offers the prospect of using ^{19}F-MRI to image tissue and organs or small-sized animal models.

As sufficient sensitivity is expected to be one of the key factors for the envisaged ^{19}F-MRI in vivo applications, we estimated the limit of detection from the signal/noise ratio obtained at different peptide concentrations (**Figure 3**). We used solution NMR to avoid that a potentially lower sensitivity of the microcoil setup used for our ^{19}F MRI would not lead to representative signal/noise values, and considered the small voxel volume observed in MRI and different signal recovery requirements inherent in the used FLASH imaging sequence in the analysis. For an order of magnitude estimate, it should be sufficient to assume that the signal scales proportionally with the sample volume, neglecting potential hardware related differences in performance. In this case we can then relate the signal obtained from a 5 mm tube using NMR spectroscopy to a generalized MRI setting which in general has a different size. As a typical ^{19}F-MRI in vivo application, we assumed the acquisition of a 2D image of a slice, as, for example, acquired in ^{19}F-MRI in vivo experiments using nanoparticle label on mice or zebrafish.[16,34] To relate the signal to noise values obtained by solution NMR of a 5 mm tube sample, we considered a 64 × 64 pixel image matrix of a slice covering 1/10 of the sample, and a FLASH sequence with a 20° flip angle (yielding 34% signal) and a typical repetition time of 10 ms.[33] (We note at this point that due to the small flip angle the repetition time of the FLASH sequence does not depend much on the T_1 relaxation time.) Taking an MRI experiment of a mouse with a field of view of 3 cm × 3 cm × 6 cm as an example, these settings would correspond to a slice thickness along the long axis of 6 mm, and a resolution of ≈470 µm × 470 µm, yielding a voxel volume of 1.3 µL. Assuming a signal/noise ratio of 5 as minimum for a detectable signal, and that the MRI signal is lower by a factor of ≈1/2000 (=1/10 × 1/64 × 0.34), a signal/noise ratio of ≈10 000 would be required in a 1D NMR spectrum of ≈1000 repetitions to correspond to the detection of an MRI 2D image within 10 min (the duration of ≈1000 repetitions of 64 spatial increments). For the longer peptides P1–P4, this limiting signal/noise ratio is reached with peptide concentrations of ≈2 mM (Figure 3). In biological tissue the signal may be reduced due to further line broadening. However, as our estimate was derived at a rather low magnetic field of 7 T (300 MHz) and many current MRI applications are performed at higher fields, the estimate of ≈1 mM peptide concentration should be a realistic figure.

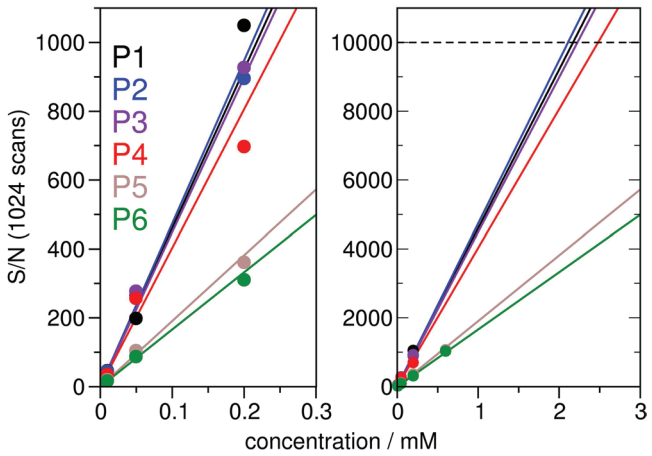

Figure 3. Estimate of the limiting concentration needed for the acquisition of an ^{19}F MRI image. The signal/noise ratios of 1024 repetitions were measured for peptides P1–P6 at different concentrations in PBS buffer (in 5 mm tubes) using solution ^{19}F NMR at 7 T (300 MHz ^{1}H resonance frequency). A signal/noise ratio of ≈10 000 (marked by a dashed line) is estimated to be sufficient to collect a ^{19}F MRI image (2D slice of 64 × 64 matrix) within 10 min.

Chemical and biological stability, as well as absence of toxicity are essential for in vivo MRI imaging applications, which was evaluated for all peptide-based labels. All peptides were found to be stable in PBS for more than one week at room temperature (Figure S17, Supporting Information). We further investigated the behavior of peptides in bovine blood serum and plasma, and observed over 60% intact peptides after 7 days incubation (**Figure 4**A and Figures S18–S20, Supporting Information). Hence, the long-term stability renders the peptides promising candidates for in vivo applications or even long-term tracking of drugs. For example, biomolecules such as antibodies tend to require an extended time to accumulate in the target tissue or organ.[35] We note at this point that the rhodamine-labeled peptides were found to degrade or co-precipitate with serum protein more rapidly (Figures S21–S23, Supporting Information), which might be related to their higher hydrophobicity. Rhodamine labeling (used here for dual-purpose fluorescent monitoring, see below) may thus alter the propensity for degradation or precipitation processes, which would however not impede any application of the peptides in ^{19}F-MRI where rhodamine labeling is obviously not needed.

To evaluate a potential toxicity in light of in vivo applications, we conducted MTT assays on HeLa and HEK293 cells for all six peptides. A viability of more than 75% in the case of HeLa cells after 24 h incubation with up to 0.1 mM of the peptides (Figure 4B) was observed. For P2, an extension of the test series to 10 mM showed a viability of 100% at 1 mM peptide concentration, which was reduced to ≈40% at 10 mM. In the case of HEK293 cells, except for P4, all peptides showed an MTT-assay signal corresponding to a cell viability of more than 80%. The MTT assay may only represent one aspect of toxicity, and give only a rough indication of limiting toxic concentrations, as it probes the influence on particular cell cultures, but not on an organism level. However, the concentrations where the peptide was still found to be non-toxic and minimum concentrations needed for ^{19}F MRI detection are within the same ballpark of roughly in the ≈1 mM range. Furthermore, the modular design allows to build peptides with different properties, such as positive or negative charge, and this way provides means to optimize for low toxicity in the desired application. Thus, the seemingly low cytotoxicity and versatile building concept of these peptides provides a good basis for in vivo ^{19}F-MRI at the cellular level.

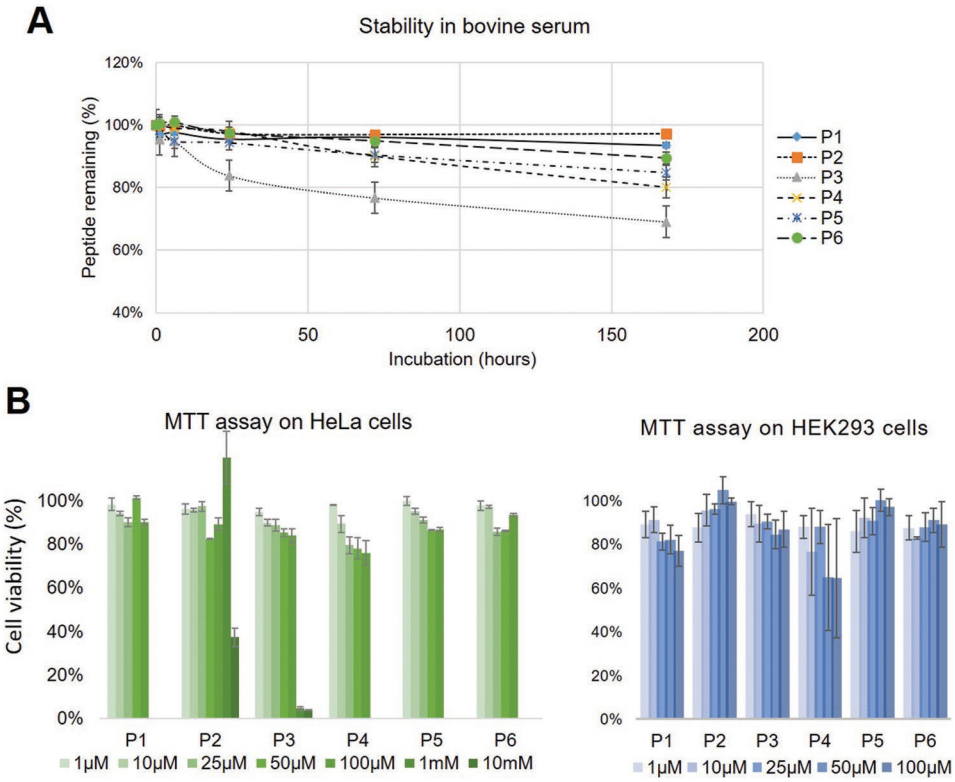

Figure 4. In vitro biological properties of the ^{19}F-peptide probes. A) Stability of peptides in bovine serum with increasing incubation time (0–7 days) at 37 °C. B) Viability of HeLa (left) and HEK293 (right) cell cultures exposed to various concentrations of peptide probes. The cell viability was obtained by monitoring the reduction of 3-(4,5-dimethylthiazol-2-yl)-2,5-diphenyltetrazolium bromide (MTT assay), where the amount of the formazan product (quantified by optical absorbance) was plotted as cell viability. 100% cell viability refers to untreated cells.

In order to assess the potential of the peptide probes for in vivo ^{19}F-MRI, we applied the rhodamine-labeled peptides (Rho-P1 to Rho-P6) to zebrafish embryos and followed their distribution and clearance using fluorescence microscopy. A 1 mg ml^{-1} Rho-peptide solution was intravenously injected into 3 day-post-fertilization (dpf) zebrafish embryos. The rhodamine-labeled peptides were observed to circulate stably in the blood stream (**Figure 5**). The absence of accumulation in the caudal vein plexus, an embryonic tissue functionally equivalent to the fetal liver in mammals, indicates that the peptides were not recognized by macrophages and scavenger endothelial cells.[36] The Rho-peptides were also observed in the anterior chamber of the eye and optic tectum in the brain, suggesting their unique ability to cross the blood–aqueous and blood–brain barrier, respectively. Notable findings are the presence of fiber-like structures in the corneal epithelium (arrowheads in Figure 5D) with Rho-P4, and large amounts of Rho-P6 along the radial glia fiber (arrowhead in Figure 5f). Furthermore, the half-life of the rhodamine-labeled peptides in the zebrafish embryo was analyzed by fitting an exponential decay (with offset) model to the fluorescence intensity change over a period of 19 h. Among the peptides, Rho-P5 and Rho-P6 had the shortest half-life of 1.75 h and the longest of 30.55 h, respectively, while Rho-P1 to Rho-P4 possess similar half-life times between 7–15 h (Figure S24, Supporting Information). In terms of biodegradation, Rho-P6 and Rho-P4, having longer lifetimes in blood circulation, are the most promising candidates as dual probes to be used in correlative ^{19}F-MRI and fluorescence imaging.

With a view to possible in vivo ^{19}F-MRI applications involving molecular targeting, we explored the coupling of the peptides to small molecules and proteins. The peptide or protein part of such bioconjugates can be chosen to possess an affinity for specific targets in the organism or specific tissue regions, then allowing, for example, molecular tracking or visualization of uptake of different body parts.[16] For a proof-of-principle validation, two thiol-containing targets, glutathione (GSH) and bovine serum albumin (BSA), were labeled using a combination of thiol-alkyne addition and copper-mediated azide-alkyne "click" chemistry. (In an in vivo application, the coupling would be performed prior administration to the organism.) We built the bridge between the alkyne function of the fluorinated peptide and the conjugation partner with commercially available 3-(4-azidophenyl)propiolonitrile (APN-azide) as cross-linker, as it has been reported that APN-based modifications avoid side products and produce conjugates that are stable in the blood stream.[37] APN-azide was attached to the peptide probe using previously described conditions,[38] and subsequently purified via RP-HPLC (**Figure 6**A, Table S3, and Figure S25, Supporting Information). Afterward, BSA and GSH were conjugated to the peptides under mild reaction conditions (in PBS at 4 °C overnight) by coupling the thiols of the cysteine residues with the second functional end of the APN linker of the peptides. GSH-conjugates were readily purified using RP-HPLC, whereas the unreacted peptide was removed by dialysis in the case of the BSA-conjugates. After validation of the bioconjugates by MALDI-MS, ^{19}F-NMR spectra

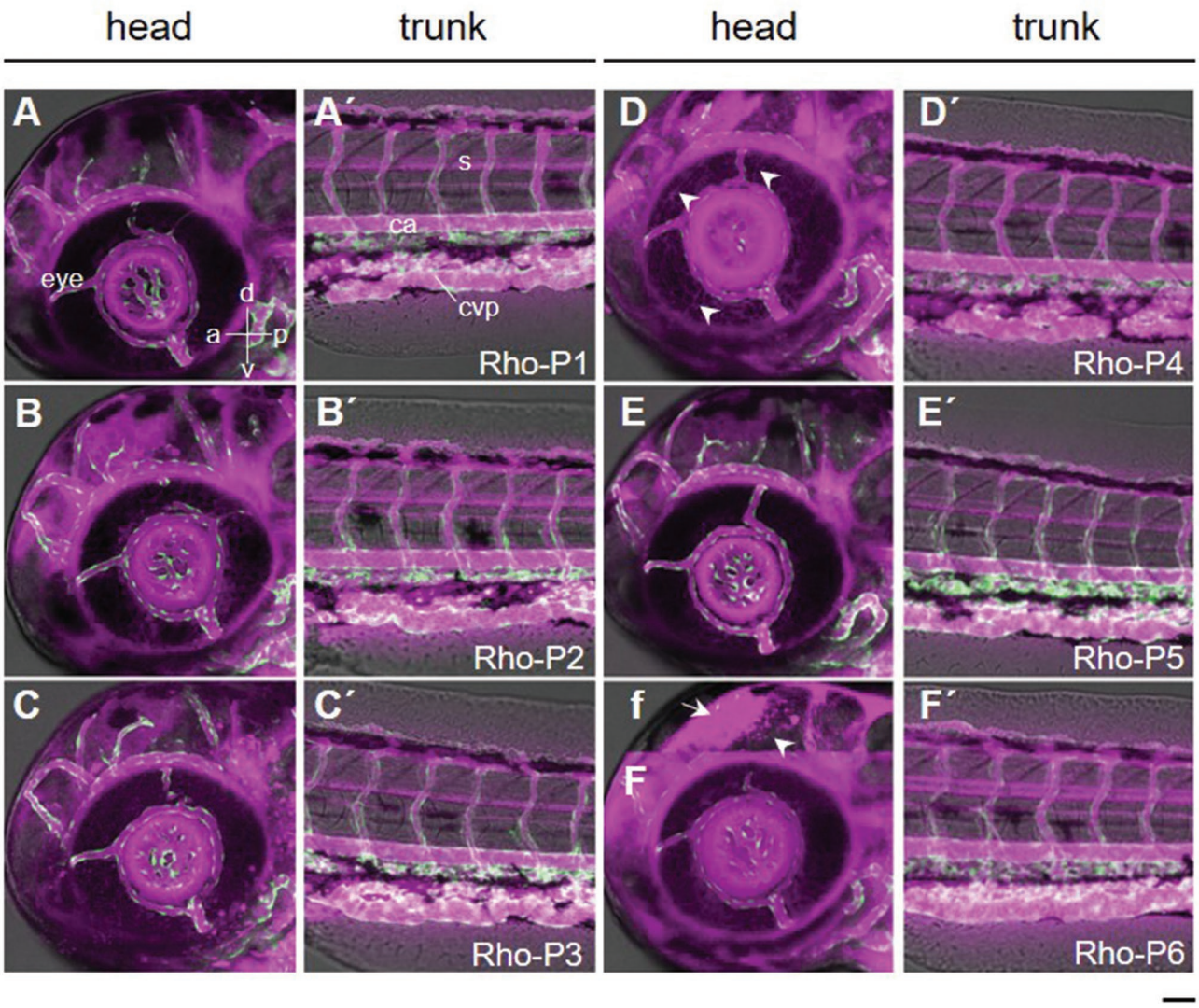

Figure 5. Biodistribution of the rhodamine labeled peptides (Rho-P1 to Rho-P6) in zebrafish embryos. A,A´) Rho-P1, B,B´) Rho-P2, C,C´)Rho-P3, D,D´) Rho-P4, E,E´) Rho-P5, and f,F,F´) Rho-P6 were intravenously injected into 3 dpf *Tg(kdrl:EGFP)s843Tg* zebrafish embryos and 3D images from the head (A–F) and trunk (A´–F´) regions were acquired every hour for 19 h ($n = 3$ embryos for each peptide). f) A single focal plane in the brain region was selected to highlight the distribution of Rho-P6 along the radial glia fiber. Images shown are from 1 h-post-injection. Peptide distribution and blood vessels are shown in magenta and green, respectively. The fluorescence microscopy images are superimposed on bright-field images (grey) from a selected single plane. Lateral views of the embryos are oriented anterior left with dorsal up. a, anterior; p, posterior; d, dorsal; v, ventral; ca, caudal artery; cvp, caudal vein plexus; s, spinal cord. Scale bar: 50 µm.

and relaxation times were acquired (Figure 6B, Figures S26–S28, and Table S4, Supporting Information). Both conjugates gave rise to a single ^{19}F-NMR signal in aqueous solution. While the chemical shift did not change significantly, the linewidth of the BSA-conjugate at half-height appears to broaden to various extents (Figure 6B, right). In the case of the GSH-conjugates, the linewidth was comparable to that of the free peptide (Figure 5B, left). Also, the relaxation times changed in the case of the BSA-conjugates, T_1 was reduced by half, and T_2 was found to be 5–20 fold shorter than that of the free peptides (Table S5, Supporting Information). Given the high molecular weight of the BSA-conjugates, these changes in relaxation behavior are in line with our predictions. Nevertheless, the ^{19}F-NMR linewidth of 16.6 Hz still lies within the range of other probes that have been used successfully in ^{19}F-MRI,[25] thus rendering also the new peptide conjugates as suitable labels for ^{19}F-MRI. Our dual-purpose peptide-based fluorine probes thus offer a general modular approach to label proteins, in order to track them via fluorescence and ^{19}F-MRI, either in parallel or subsequently. The APN-based cross-linker can be easily changed to functionalities other than thiols, if further types of functional groups are to be targeted.

3. Conclusion

In conclusion, we have designed, synthesized, and characterized highly fluorinated peptide probes for ^{19}F-MRI. Introducing an asparagine analogue carrying a perfluoro-*tert*-butyl group as

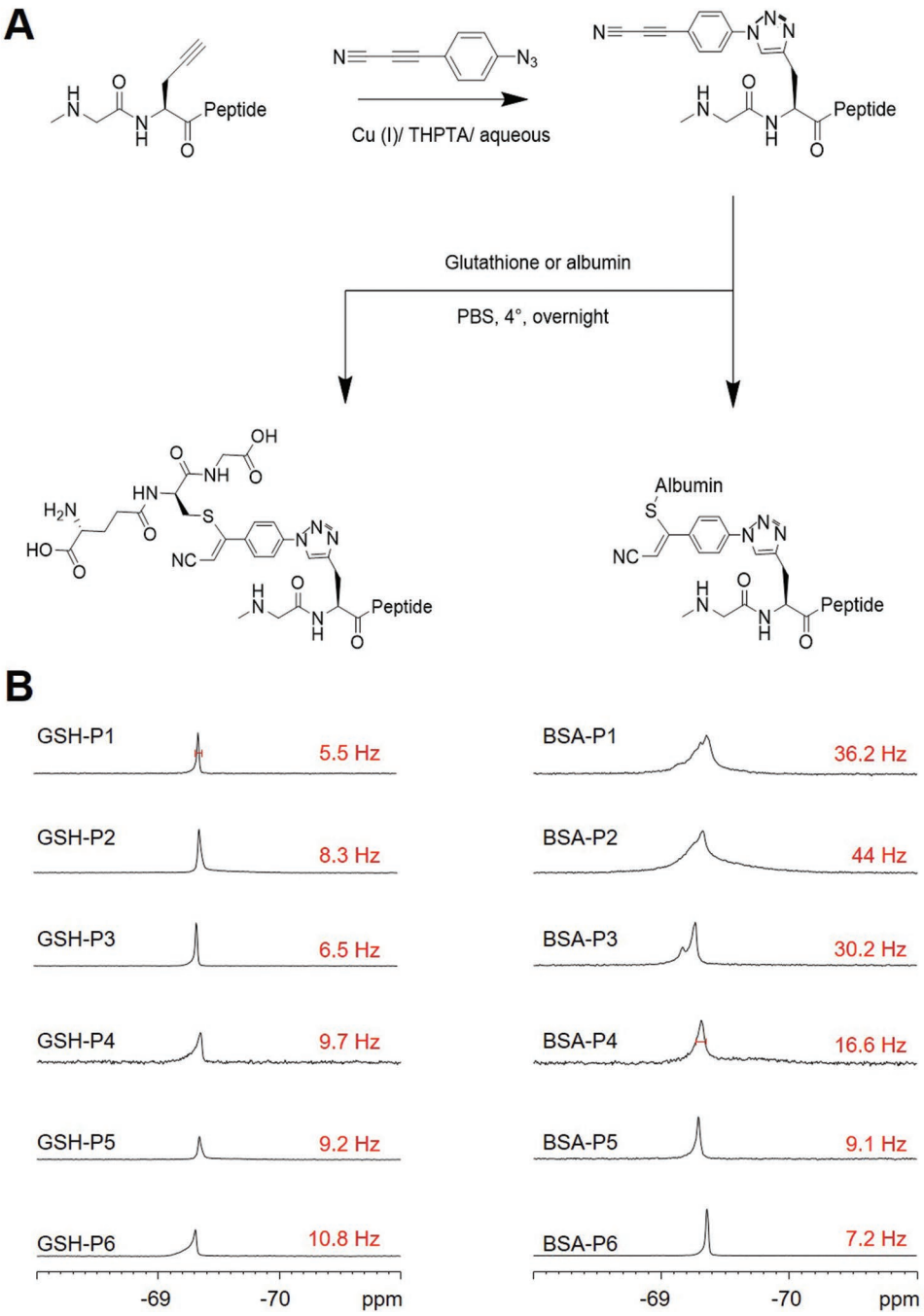

Figure 6. Conjugation of fluorinated peptides with biomolecules, and ^{19}F-NMR spectra of conjugates with GSH and BSA. A) Coupling of the peptides to a cross-linker via copper-catalyzed "click" reaction, followed by thiol conjugation with BSA and GSH in PBS. B) GSH-peptides and BSA-peptides in PBS were characterized using ^{19}F-NMR. Peak linewidths at half height are indicated.

fluorine label into peptides, as well as D-stereoisomers of charged amino acids, we were able to design MRI probes endowed with high water solubility and stability against degradation. Due to our design of the peptide sequence—which avoids secondary structure formation and which is based on equal repeat units—a dispersion of ^{19}F chemical shifts could be prevented and high intensity and small linewidth were achieved. Low cytotoxicity, high biostability, and tissue penetration have been demonstrated in cell assays and live zebrafish embryos, and stable bioconjugates could be achieved with BSA and GSH. Hence, optimized ^{19}F-NMR signal and biocompatibility render the Asn^{F9} based peptide probes highly promising candidates for in vivo applications of ^{19}F-MRI.

4. Experimental Section

Synthetic Procedures: Details of the synthesis and chemical analysis of the fluorine-labeled amino acid and the peptides are given in the Supporting Information.

^{19}F-NMR and Relaxation Time Measurements: Liquid-state ^{19}F-NMR spectra were obtained using a 300 MHz Bruker Avance spectrometer (Bruker Biospin, Ettlingen) with a multiple channel (^{1}H/^{2}H/^{19}F/^{13}C/^{15}N) probe. Peptide samples were dissolved in methanol and phosphate buffered saline (PBS) buffer with pH 7.4. The ^{19}F-NMR spectra were acquired using a single excitation pulse sequence of 15 µs and an acquisition time of 0.66 s. Around 1000 scans, separated by a recycle delay of 3 s, were averaged. The ^{19}F-NMR spectra were referenced indirectly using the ^{1}H-NMR signal of the solvent (methanol, set to 4.78 and 3.31 ppm, or H_2O, set to 4.8 ppm) and processed using a line broadening of 1 Hz. All measurements were performed at room temperature (20 °C). The ^{19}F-NMR spin-lattice relaxation time T_1 was acquired using the inversion recovery method with delay times of 0.000001, 0.01, 0.02, 0.05, 0.1, 0.2, 0.5, 1, 2, 5, and 10 s. Eleven spectra were obtained using a 90°-pulse of 15 µs and a recycle delay of 10 s. ^{19}F-NMR spin–spin relaxation times T_2 were acquired using a Hahn echo sequence with delay times of 0.00001, 0.001, 0.002, 0.005, 0.010, 0.020, 0.050, 0.1, 0.2, 0.5, 1, and 2 s. Twelve spectra were obtained using a 90°-pulse of 15 µs and a recycle delay of 5 s. Approximately 36–64 scans were accumulated in the T_1 and T_2 experiments. T_1 and T_2 relaxation times were analyzed using the relaxation fitting functions within the software Topspin 4.1.1 (Bruker).

MRI: ^{19}F-MRI images were obtained using a 500 MHz Bruker Avance III widebore spectrometer (Bruker Biospin, Ettlingen). Peptides were dissolved in 6 mM $CuSO_4$ using a peptide concentration corresponding to a ^{19}F concentration of 675 mM. 65 mM NaOH was added to the solutions of P1 and P2 to improve solubility. The peptide solutions were filled in one side sealed capillaries with inner diameter of 1.6 mm and outer diameter of 2.0 mm. The capillaries were then inserted into a 2.2 mm inner diameter glass tube surrounded by a custom-made dual-tuned ^{1}H/^{19}F micro saddle coil.[32] Experiments were carried out at 20 °C with an external water flow for cooling the gradient coils. ^{19}F-MRI of the peptides was carried out using a FLASH sequence with adjusted parameters (echo time: 2.72 ms, repetition time: 5.76 ms, flip angle = 45°, image size: 32 × 32 pixels, field of view: 7 × 7 mm, resolution 0.219 × 0.219 mm, slice sickness: 1 mm). Images were obtained of coronal planes and averaged over 10 000 scans. Images were acquired using the ParaVision 6.0.1 software and post-processed using pixel binning (averaging shrink factor of 32) by Fiji/ImageJ.

Digestion Assay: The stability of the peptides was assessed using an assay based on digestion in bovine serum and bovine plasma. As a first step, commercial fetal bovine serum was temperature-equilibrated at 37 °C for 15 min. 0.6 mg of peptide in 100 µL of PBS buffer (pH 7.4) was added to the serum to a final concentration of 50 mM. At 0, 1, 6, 24, 72, and 168 h, 100 µL aliquots were taken and mixed with 500 µL MeOH for 20 min on ice. Serum proteins were precipitated and removed by centrifugation at 13 000 rpm for 15 min. The supernatant was immediately analyzed by analytical RP-HPLC using a linear gradient of solvent A/B ratios of 5:95—95:5 in 25 min (A: 97% H_2O, 3% ACN, 0.1% TFA; B: 90% ACN, 10% H_2O, 0.1% TFA), or stored in –80 °C freezer for further analysis. The measurements were carried out three times. The digestion assay in bovine plasma was performed using the same procedure.

Cytotoxicity Assay: A MTT assay on HeLa cells and HEK 293 cells was carried out to evaluate the toxicity of the peptides. Cells were plated in 96-well plates at a density of 15 000 cells per well and grown overnight. Before adding the peptide solutions, the previous cell media were discarded and incubated with DMEM pure for 30 min. The adherent cells were washed with PBS. The peptide solutions were then successively added into 96-well plates, and filled up with pure DMEM to the working volume of 200 µL. After the incubation of the plate at 37 °C for 24 h, 100 µL MTT solution was added to the washed cell and incubated for 2–4 h until the visibility of purple formazan. Afterward, MTT solutions were removed and cells were washed with PBS. 100 µL DMSO was added into each well to dissolve the purple crystals. The optical densities were measured at 570 nm and the value of a blank sample was subtracted. Assays were carried out three times.

Zebrafish Experiments: All zebrafish husbandry and experiments were performed in accordance with the German animal protection regulations. *Danio rerio* transgenic line Tg(kdrl:EGFP)s843Tg was used to visualize blood vessels. Embryos were maintained at 28 °C as previously described.[39]

Intravenous Peptide Injection: Zebrafish embryos at 3 dpf were anesthetized in 643 µM MS-222 (tricaine methanesulfonate) and embedded in 0.8% low melting-agarose. Rhodamine B labeled peptides were dissolved in PBS buffer (pH 7.4) at a concentration of 1 mg mL^{-1} (0.5 mM for P1–P4 and 1.3 mM for P5–P6, respectively). A few microliters of peptide solution were transferred into a pulled glass capillary and 10–20 nL was injected into the cardinal vein by a micro-injector (Eppendorf FemtoJet) at room temperature.

Fluorescence Imaging: Injected embryos were observed under a Leica TCS SP5 upright confocal microscope (Leica Microsystems) with excitation lasers at 488 and 561 nm for the detection of EGFP (498–528 nm) and rhodamine B (574–634 nm), respectively. Bright field transmission images were also acquired. A "HCX APO L U-V-I 20.0 × 0.50 WATER UV" objective lens was used. Time-lapse imaging in the head and trunk regions of the zebrafish embryos was performed using the resonant scanning mode of the microscope (bidirectional scanning at 8000 Hz) for 18 embryos injected with six different peptides, repeating the measurement three times for each peptide. The images were analyzed by Fiji/ImageJ.

Supporting Information

Supporting Information is available from the Wiley Online Library or from the author.

Acknowledgements

The authors acknowledge the financial support by the strategy fund of KIT (division 1), by the DFG instrument grant 121384/58-1, by the GRK 2039 programme, by EU H2020-MSCA-RISE through the PELICO (grant 690973) and ALISE (grant 101007256) projects, and by BMBF through the VIP+ funding. The authors thank Markus Schmitt for technical support and Ronja Kammerichs for help in cell experiments. The MRI measurements were supported by the Karlsruhe Nano and Micro Facility (KNMFi), a Helmholtz Research Infrastructure at KIT. N.M., O.N., and J.G.K. acknowledge partial financial support of the Helmholtz Association through the programme "Materials Systems Engineering" and through the ERC Synergy Grant "HiSCORE" 951459, while S.L.G., S.A., M.T., and A.S.U. are part of the programme "Natural, Artificial, and Cognitive Information Processing."

Open access funding enabled and organized by Projekt DEAL.

Conflict of Interest

The authors declare no conflict of interest.

Data Availability Statement

The data that support the findings of this study are available from the corresponding author upon reasonable request.

Keywords

^{19}F-MRI, bioconjugation, fluorescence imaging, highly fluorinated peptides, perfluoro-*tert*-butyl amino acid, zebrafish embryos

Received: November 25, 2021
Revised: July 29, 2022
Published online:

[1] J. Wang, M. Sánchez-Roselló, J. L. Aceña, C. del Pozo, A. E. Sorochinsky, S. Fustero, V. A. Soloshonok, H. Liu, *Chem. Rev.* **2014**, *114*, 2432.
[2] B. G. de la Torre, F. Albericio, *Molecules* **2019**, *24*, 809.
[3] B. G. de la Torre, F. Albericio, *Molecules* **2020**, *25*, 745.
[4] K. Haranahalli, T. Honda, I. Ojima, *J. Fluorine Chem.* **2019**, *217*, 29.
[5] H.-J. Böhm, D. Banner, S. Bendels, M. Kansy, B. Kuhn, K. Müller, U. Obst-Sander, M. Stahl, *ChemBioChem* **2004**, *5*, 637.
[6] I. V. Komarov, S. Afonin, A. S. Ulrich, in *Fluorine in Life Sciences: Pharmaceuticals, Medicinal diagnostics, and Agrochemicals* (Eds: G. Haufe, F. R. Leroux), Academic Press, Cambridge, MA **2019**, pp. 349–395.
[7] D. Gimenez, A. Phelan, C. D. Murphy, S. L. Cobb, *Beilstein J. Org. Chem.* **2021**, *17*, 293.
[8] P. Wadhwani, J. Reichert, E. Strandberg, J. Burck, J. Misiewicz, S. Afonin, N. Heidenreich, S. Fanghanel, P. K. Mykhailiuk, I. V. Komarov, A. S. Ulrich, *Phys. Chem. Chem. Phys.* **2013**, *15*, 8962.
[9] L. Ye, N. Van Eps, M. Zimmer, O. P. Ernst, R. S. Prosser, *Nature* **2016**, *533*, 265.
[10] J. D. Seitz, J. G. Vineberg, L. Wei, J. F. Khan, B. Lichtenthal, C. F. Lin, I. Ojima, *J. Fluorine Chem.* **2015**, *171*, 148.
[11] W. S. H. G. N. Holland, P. A. Bottomley, *J. Magn. Reson.* **1977**, *28*, 133.
[12] M. A. Miller, E. M. Sletten, *ChemBioChem* **2020**, *21*, 3451.
[13] E. A. Waters, J. Chen, J. S. Allen, H. Zhang, G. M. Lanza, S. A. Wickline, *J. Cardiovasc. Magn. Reson.* **2008**, *10*, 43.
[14] U. Flogel, Z. Ding, H. Hardung, S. Jander, G. Reichmann, C. Jacoby, R. Schubert, J. Schrader, *Circulation* **2008**, *118*, 140.
[15] F. Chapelin, C. M. Capitini, E. T. Ahrens, *J. Immunother. Cancer* **2018**, *6*, 105.
[16] K. Akazawa, F. Sugihara, T. Nakamura, H. Matsushita, H. Mukai, R. Akimoto, M. Minoshima, S. Mizukami, K. Kikuchi, *Angew. Chem., Int. Ed.* **2018**, *57*, 16742.
[17] C. Zhang, L. Li, F. Y. Han, X. Yu, X. Tan, C. Fu, Z. P. Xu, A. K. Whittaker, *Small* **2019**, *15*, 1902309.
[18] H. Lin, X. Tang, A. Li, J. Gao, *Adv. Mater.* **2021**, *33*, 2005657.
[19] M. H. Cho, S. H. Shin, S. H. Park, D. K. Kadayakkara, D. Kim, Y. Choi, *Bioconjugate Chem.* **2019**, *30*, 2502.
[20] Y. Li, J. Cui, C. Li, H. Zhou, J. Chang, O. Aras, F. An, *ChemMedChem* **2022**, *17*, 202100701.
[21] J. Ruiz-Cabello, B. P. Barnett, P. A. Bottomley, J. W. Bulte, *NMR Biomed.* **2011**, *24*, 114.
[22] E. A. Tanifum, C. Patel, M. E. Liaw, R. G. Pautler, A. V. Annapragada, *Sci. Rep.* **2018**, *8*, 2889.
[23] S. E. Kirberger, S. D. Maltseva, J. C. Manulik, S. A. Einstein, B. P. Weegman, M. Garwood, W. C. K. Pomerantz, *Angew. Chem., Int. Ed.* **2017**, *56*, 6440.
[24] B. C. Buer, B. J. Levin, E. N. Marsh, *J. Pept. Sci.* **2013**, *19*, 308.
[25] N. G. Taylor, S. H. Chung, A. L. Kwansa, R. R. JohnsonIII, A. J. Teator, N. J. B. Milliken, K. M. Koshlap, Y. G. Yingling, Y. Z. Lee, F. A. Leibfarth, *Chem. - Eur. J.* **2020**, *26*, 9982.
[26] C. M. Tressler, N. J. Zondlo, *Biochemistry* **2017**, *56*, 1062.
[27] C. M. Tressler, N. J. Zondlo, *Org. Lett.* **2016**, *18*, 6240.
[28] C. M. Tressler, N. J. Zondlo, *J. Org. Chem.* **2014**, *79*, 5880.
[29] J. J. Kasper, J. E. Hitro, S. R. Fitzgerald, J. M. Schnitter, J. J. Rutowski, J. A. Heck, J. L. Steinbacher, *J. Org. Chem.* **2016**, *81*, 8095.
[30] S. Abirami, Y. M. Xing, C. W. Tsang, N. L. Ma, *J. Phys. Chem. A* **2005**, *109*, 500.
[31] M. Beija, C. A. M. Afonso, J. M. G. Martinho, *Chem. Soc. Rev.* **2009**, *38*, 2410.
[32] O. Nassar, M. Jouda, M. Rapp, D. Mager, J. G. Korvink, N. MacKinnon, *Microsyst. Nanoeng.* **2021**, *7*, 30.
[33] A. Haase, J. Frahm, D. Matthaei, W. Hänicke, K.-D. Merboldt, *J. Magn. Reson.* **1986**, *67*, 258.
[34] Y. Yuan, S. Ge, H. Sun, X. Dong, H. Zhao, L. An, J. Zhang, J. Wang, B. Hu, G. Liang, *ACS Nano* **2015**, *9*, 5117.
[35] Z. Li, B. F. Krippendorff, S. Sharma, A. C. Walz, T. Lavé, D. K. Shah, *mAbs* **2016**, *8*, 113.
[36] Y. Hayashi, M. Takamiya, P. B. Jensen, I. Ojea-Jiménez, H. Claude, C. Antony, K. Kjaer-Sorensen, C. Grabher, T. Boesen, D. Gilliland, C. Oxvig, U. Strähle, C. Weiss, *ACS Nano* **2020**, *14*, 1665.
[37] O. Koniev, G. Leriche, M. Nothisen, J. S. Remy, J. M. Strub, C. Schaeffer-Reiss, A. Van Dorsselaer, R. Baati, A. Wagner, *Bioconjugate Chem.* **2014**, *25*, 202.
[38] Y. H. Lau, Y. Wu, P. de Andrade, W. R. Galloway, D. R. Spring, *Nat. Protoc.* **2015**, *10*, 585.
[39] M. Westerfield, *The Zebrafish Book. A Guide for the Laboratory Use of Zebrafish (Danio rerio)*, 4th ed., University of Oregon Press, Eugene, OR **2000**, p. 300.